Article:
Khamas, S.K. (2010) Asymptotic extraction approach for antennas in a multilayered spherical media. IEEE Transactions on Antennas and Propagation, 58 (3). pp. 1003-1008. ISSN: 0018-926X

https://doi.org/10.1109/TAP.2009.2039333

Asymptotic Extraction Approach for Antennas in a Multilayered Spherical Media

Salam K. Khamas

***Abstract*—An efficient algorithm is introduced to enhance the convergence of dyadic Green's functions (DGF) in a layered spherical media where asymptotic expressions have been developed. The formulated expressions involve an infinite series of spherical eigenmodes that can be reduced to the simple homogenous media Green's function using the addition theorem of spherical Hankel functions. Substantial improvements in the convergence speed have been attained by subtracting the asymptotic series representation from the original DGF. The subtracted components are then added to the solution using the homogenous media Green's function format.**

***Index Terms*—Dyadic Green's function, method of moments, spherical antennas.**

I. Introduction

Rigorous analysis of electromagnetic waves' radiation and scattering in the presence of a layered dielectric sphere has been reported in a number of studies [1]–[4], where the required dyadic Green's function has been expressed in the form of an infinite series of spherical eigenmodes. This series is convergent and hence can be truncated using a finite number of terms. However, the convergence speed depends on a number of factors such as sphere radius, permittivity and the distance between the source and field points, $\mathbf{r}'$ and $\mathbf{r}$, respectively. A large number of terms must be added in the summation when $\mathbf{r}'$ and $\mathbf{r}$ are in the vicinity of each other and both are in the proximity of a dielectric interface. Once the source and the observation points are apart from an interface, convergence of the series can be achieved using a considerably reduced number of terms.

Accelerating the infinite summation convergence can produce a computationally faster model. Furthermore, a common concern with adding a larger number of terms is the requirement to compute the spherical Hankel and Bessel functions, $h_n(kr)$ and $j_n(kr)$, of large orders. This is generally known to be accompanied by numerical over flows, or under flows; hence, it may result in a potentially unstable model. Several studies on speeding up the convergence are available in the literature using Watson [5] or Shanks [6], [7] transformations, where the former cannot be used when the source and field points are on the same radial line [7] and the latter needs additional numerical considerations. Further, the required DGF expansion coefficients poles need to be determined numerically for a multilayered structure when Watson transformation is used [8], which increases the complexity of the model. An alternative approach to reduce the required number of summation terms has been reported in [8], where a closed-form representation of the Green's function has been attained using finite difference algorithm to model the layered sphere. This approach enhances the computation efficiency as the angular distance between source and field points increases. Other solutions have been reported in [9], [10] to accelerate convergence in the case of a radial monopole above, or connected, to a large PEC sphere. However, those solutions cannot be adopted in the presence of conformal current sources or for layered spherical structures. A different approach to reduce the computation time has been proposed in [11], [12] through the development of novel closed-form expressions for the required numerical integrations in a method of moments (MoM) solution.

A well-known technique that has been employed in the analysis of planar and cylindrical geometries is the asymptotic extraction approach [13]–[16], where the quasi-static images are extracted from the Sommerfeld-type integrals and then added back to the overall Green's function using closed-form representations. In this article, the asymptotic extraction is adopted for spherical structures to expedite the infinite series convergence. This is based on developing asymptotic expressions for the DGF components as the summation index approaches infinity. These expressions have been incorporated into a new infinite series that can be expressed in a closed form by employing the spherical Hankel function addition theorem. A rapidly convergent model is then accomplished by subtracting the new series from the original summation. The subtracted series was subsequently added, albeit in a closed form, to the overall DGF expression. A method of moments model has been developed by adopting the introduced procedure, where it was found that the convergence speed is accelerated by several folds while accuracy is maintained.

II. Formulation

Fig. 1 illustrates a layered sphere that consists of four layers where each layer has a permittivity of ε_f and a permeability of μ_f. The source and the field points could be located in any layer. For an antenna radiating in the vicinity of such a sphere, the DGF may be expressed as [1]–[3]

$$\overline{\mathbf{G}}_e^{fs}(\mathbf{r},\mathbf{r}') = \left(\bar{\mathbf{I}} + \frac{1}{k_f^2}\nabla\nabla'\right)\frac{e^{-jk_fR}}{4\pi R}\delta_f^s + \overline{\mathbf{G}}_{es}^{(fs)}(\mathbf{r},\mathbf{r}') \quad (1)$$

where the superscript fs refers to the layers of field and source points. The first term represents the DGF component owing to antenna radiating in an infinite homogenous media, while the second term is the scattering DGF that accounts for the presence of a layered sphere, given by [3]

$$\begin{aligned}\overline{\mathbf{G}}_{es}^{(fs)}&(\mathbf{r},\mathbf{r}') \\ &= \frac{jk_s}{4\pi}\sum_{n=0}^{\infty}\sum_{m=0}^{n}\left(2-\delta_m^0\right)\frac{2n+1}{n(n+1)}\frac{(n-m)!}{(n+m)!} \\ &\quad\times\left\{\Delta_1\mathbf{M}_{mn}^{(2)}(k_f)\left(\Delta_2 A_M^{fs}\mathbf{M}'_{mn}(k_s)+\Delta_3 B_M^{fs}\mathbf{M}'^{(2)}_{mn}(k_s)\right)\right. \\ &\qquad+\Delta_1\mathbf{N}_{mn}^{(2)}(k_f)\left(\Delta_2 A_N^{fs}\mathbf{N}'_{mn}(k_s)+\Delta_3 B_N^{fs}\mathbf{N}'^{(2)}_{mn}(k_s)\right) \\ &\qquad+\Delta_4\mathbf{M}_{mn}(k_f)\left(\Delta_2 C_M^{fs}\mathbf{M}'_{mn}(k_s)+\Delta_3 D_M^{fs}\mathbf{M}'^{(2)}_{mn}(k_s)\right) \\ &\qquad\left.+\Delta_4\mathbf{N}_{mn}(k_f)\left(\Delta_2 C_N^{fs}\mathbf{N}'_{mn}(k_s)+\Delta_3 D_N^{fs}\mathbf{N}'^{(2)}_{mn}(k_s)\right)\right\}\end{aligned} \quad (2)$$

where $\mathbf{M}_{mn}$ and $\mathbf{N}_{mn}$ are the well-known spherical vector eigenfunctions of the transverse electric, TE_{mn}, and transverse magnetic, TM_{mn}, modes, respectively, the superscript (2) refers to the second type spherical Hankel functions, $\Delta_1 = \left(1-\delta_f^L\right)$, $\Delta_2 = \left(1-\delta_s^1\right)$, $\Delta_3 = \left(1-\delta_s^L\right)$, $\Delta_4 = \left(1-\delta_f^1\right)$, δ_u^v is the Kronecker delta, and L is

Manuscript received May 20, 2009; revised August 20, 2009. First published December 31, 2009; current version published March 03, 2010.

The author is with the Communications Research Group, Department of Electronic and Electrical Engineering, University of Sheffield, Sheffield S1 3JD, U.K. (e-mail: s.khamas@sheffield.ac.uk).

Color versions of one or more of the figures in this communication are available online at http://ieeexplore.ieee.org.

Digital Object Identifier 10.1109/TAP.2009.2039333

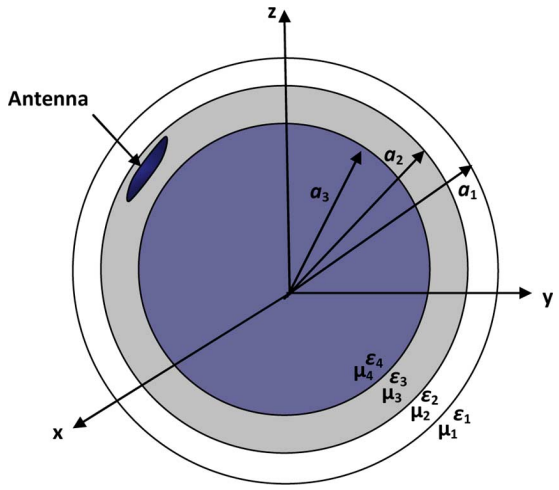

Fig. 1. Four layers dielectric sphere.

the number of spherical layers. Explicit expressions for the scattering DGF coefficients $A^{fs}_{M,N}$, $B^{fs}_{M,N}$, $C^{fs}_{M,N}$ and $D^{fs}_{M,N}$ are reported in [3].

The proposed model has been formulated by deriving asymptotic reflection and transmission coefficients to obtain the required scattering DGF coefficients, which are used to achieve the final asymptotic DGF, $\overline{\mathbf{G}}^{(fs)}_{es}\Big|_a$, where the subscript a denotes an asymptotic expression. Non magnetic materials have been considered, that is, $\mu_f = \mu_o$. However, the presented procedure can be extended to model magnetic materials with no difficulty.

A. Asymptotic Expansion Coefficients

The development of asymptotic expressions for the equivalent reflections and transmission coefficients between dielectric spherical layers is an essential step toward the accomplishment of an asymptotic DGF. Detailed expressions of these coefficients are reported in [3, Eq. (18)]. The principal form asymptotic Bessel and Hankel functions formulas given in Appendix A have been employed through the substitution of (A8) and (A9) in the reflection and transmission coefficients to attain the following:

$$R^H_{Pf}\Big|_a \approx 0 \tag{3a}$$

$$R^H_{Ff}\Big|_a \approx 0 \tag{3b}$$

$$R^V_{Pf}\Big|_a \approx -\left\{\frac{\varepsilon_{f+1}-\varepsilon_f}{\varepsilon_{f+1}+\varepsilon_f}\right\}\frac{h^{(2)}_n(k_f a_f)}{j_n(k_f a_f)} \tag{3c}$$

$$R^V_{Ff}\Big|_a \approx -\left\{\frac{\varepsilon_{f+1}-\varepsilon_f}{\varepsilon_{f+1}+\varepsilon_f}\right\}\frac{j_n(k_f a_f)}{h^{(2)}_n(k_f a_f)} \tag{3d}$$

$$T^H_{Pf}\Big|_a \approx \frac{j_n(k_{f+1}a_f)}{j_n(k_f a_f)} \tag{3e}$$

$$T^H_{Ff}\Big|_a \approx \frac{h^{(2)}_n(k_{f+1}a_f)}{h^{(2)}_n(k_f a_f)} \tag{3f}$$

$$T^V_{Pf}\Big|_a \approx -\left\{\frac{2\sqrt{\varepsilon_f\varepsilon_{f+1}}}{\varepsilon_{f+1}+\varepsilon_f}\right\}\frac{j_n(k_{f+1}a_f)}{j_n(k_f a_f)} \tag{3g}$$

$$T^V_{Ff}\Big|_a \approx -\left\{\frac{2\sqrt{\varepsilon_f\varepsilon_{f+1}}}{\varepsilon_{f+1}+\varepsilon_f}\right\}\frac{h^{(2)}_n(k_{f+1}a_f)}{h^{(2)}_n(k_f a_f)}. \tag{3h}$$

The asymptotic scattering DGF coefficients $A^{fs}_{M,N}\Big|_a$, $B^{fs}_{M,N}\Big|_a$, $C^{fs}_{M,N}\Big|_a$, and $D^{fs}_{M,N}\Big|_a$ can be determined by substituting the coefficients of (3) in the accordant expressions given in Appendix B. When both the source and field points are in the same layer, then, without loss of generality, it can be shown that

$$A^{ii}_M\Big|_a = B^{ii}_M\Big|_a = C^{ii}_M\Big|_a = D^{ii}_M\Big|_a \approx 0 \tag{4}$$

$$A^{ii}_N\Big|_a = D^{ii}_N\Big|_a \approx 0 \tag{5}$$

$$B^{ii}_N\Big|_a = -w_i\frac{j_n(k_i a_i)}{h^{(2)}_n(k_i a_i)} - w_{i+1}\frac{j_n(k_i a_{i+1})}{h^{(2)}_n(k_i a_{i+1})} \quad i < L \tag{6}$$

$$C^{ii}_N\Big|_a = -w_{i-1}\frac{h^{(2)}_n(k_i a_{i-1})}{j_n(k_i a_{i-1})} - w_{i-2}\frac{h^{(2)}_n(k_i a_{i-2})}{j_n(k_i a_{i-2})} \quad i > 1 \tag{7}$$

where $B^{LL}_N\Big|_a = C^{11}_N\Big|_a = 0$ [3], $w_i = (\varepsilon_i - \varepsilon_{i+1})/(\varepsilon_i + \varepsilon_{i+1})$, $w_{i+1} = \left(1-\delta_i^{L-1}\right)(\varepsilon_{i+1}-\varepsilon_{i+2})/(\varepsilon_{i+1}+\varepsilon_{i+2})$, $w_{i-1},= (\varepsilon_i - \varepsilon_{i-1})/(\varepsilon_i+\varepsilon_{i-1})$, and $w_{i-2} = \left(1-\delta_i^2\right)(\varepsilon_{i-1}-\varepsilon_{i-2})/(\varepsilon_{i-1}+\varepsilon_{i-2})$. Local reflections at interfaces in the vicinity of the ith layer have been considered because reflections from distant boundaries and multiple reflections decay rapidly as n increases; hence, they have no contribution to the DGF coefficients in (4)–(7). Furthermore, the TE modes coefficients asymptote to zero for larger n, while the corresponding TM modes coefficients depend on the wave reflections at the dielectric interfaces.

B. Asymptotic Dyadic Green's Functions

The asymptotic DGF components can be accomplished by substituting the coefficients given in (4)–(7) in the scattering DGF expression given by (2). For example, $G_{rr}|_a$ can be derived as

$$G_{rr}|_a = \frac{jk_i}{4\pi}\sum_{n=0}^{\infty}(2n+1)\,n\,(n+1)\frac{\xi(r,r')}{rr'k_i^2}P_n(\cos\gamma) \tag{8}$$

where $\xi(r,r') = B^{ii}_N\Big|_a h_n(k_i r')\,h_n(k_i r) + C^{ii}_N\Big|_a j_n(k_i r')\,j_n(k_i r)$, $P_n(\cos\gamma)$ is the Legendre polynomial of degree n, and $\cos\gamma = \cos\theta\cos\theta' + \sin\theta\sin\theta'\cos(\phi-\phi')$. The double summation of (2) has been reduced to a single summation using the addition theorem of Legendre polynomial [4]. Employing (A5)–(A6) and assuming $(n+1)\approx n$ for larger n, $G_{rr}|_a$ can be written in a more convenient form as

$$G_{rr}|_a = \frac{j}{4\pi k_i}\frac{\partial^2}{\partial r\partial r'}\sum_{n=0}^{\infty}(2n+1)\xi(r,r')P_n(\cos\gamma). \tag{9}$$

The other asymptotic DGF components can be derived in the same way as the component given in (9), and then incorporated into the following unified expression:

$$\begin{aligned}\overline{\mathbf{G}}^{ii}_{es}\Big|_a = {} & \frac{-j}{4\pi k_i}\nabla\nabla'\sum_{n=0}^{\infty}(2n+1)P_n(\cos\gamma)\\ & \times\left\{\left(w_i\frac{j_n(k_i a_i)}{h^{(2)}_n(k_i a_i)} + w_{i+1}\frac{j_n(k_i a_{i+1})}{h^{(2)}_n(k_i a_{i+1})}\right)\right.\\ & \times h^{(2)}_n(k_i r)\,h^{(2)}_n(k_i r')\\ & + \left(w_{i-1}\frac{h^{(2)}_n(k_i a_{i-1})}{j_n(k_i a_{i-1})} + w_{i-2}\frac{h^{(2)}_n(k_i a_{i-2})}{j_n(k_i a_{i-2})}\right)\\ & \left.\times j_n(k_i r)\,j_n(k_i r')\right\}.\end{aligned} \tag{10}$$

With the aid of (A1)–(A2), (10) may be expressed as

$$\overline{\mathbf{G}}_{es}^{ii}\Big|_a = \frac{-j}{4\pi k_i}\nabla\nabla'\sum_{n=0}^{\infty}(2n+1)P_n(\cos\gamma) \times\Bigg\{\left(w_i\frac{a_i}{r}j_n(k_i d_i)+w_{i+1}\frac{a_{i+1}}{r}j_n(k_i d_{i+1})\right)\times h_n^{(2)}(k_i r')+\left(w_{i-1}\frac{a_{i-1}}{r}h_n^{(2)}(k_i d_{i-1}) + w_{i-2}\frac{a_{i-2}}{r}h_n^{(2)}(k_i d_{i-2})\right)j_n(k_i r')\Bigg\} \quad (11)$$

where $d_\ell = \left(a_\ell^2/r\right)$. By invoking the addition theorem of the spherical Hankel function [4], (11) reduces to

$$\overline{\mathbf{G}}_{es}^{ii}\Big|_a = \frac{1}{4\pi k_i^2}\nabla\nabla'\sum_{\ell=i-2}^{i+1} w_\ell\frac{a_\ell}{r}\frac{e^{-jk_i R_\ell}}{R_\ell} \quad (12)$$

where $R_\ell = \sqrt{r'^2 + d_\ell^2 - 2r'd_\ell\cos\gamma}$.

Therefore (1) can be expressed in a computationally efficient format as

$$\overline{\mathbf{G}}_e^{ii}(\mathbf{r},\mathbf{r}') = \left\{\bar{\mathbf{I}}\frac{e^{-jk_i R}}{4\pi R}+\nabla\nabla' G\right\}+\left\{\overline{\mathbf{G}}_{es}^{ii}(\mathbf{r},\mathbf{r}')-\overline{\mathbf{G}}_{es}^{ii}\Big|_a\right\} \quad (13)$$

where

$$G = \frac{1}{4\pi k_i^2}\left(\frac{e^{-jk_i R}}{R}+\sum_{\ell=i-2}^{i+1} w_\ell\frac{a_\ell}{r}\frac{e^{-jk_i R_\ell}}{R_\ell}\right) \quad (14)$$

and $\overline{\mathbf{G}}_{es}^{ss}\big|_a$ is given by (11).

III. Results

To illustrate the significance of the presented procedure a moment method model has been developed for the analysis of spherically conformal antennas. The geometry of Fig. 1 has been modeled assuming the innermost layer to be a perfectly conducting, PEC, spherical core, the third layer is a dielectric substrate and the second layer is a spherical superstrate with the outermost layer represents free space.

As an example, a conformal Archimedean spiral antenna printed on a grounded dielectric spherical substrate has been considered [17]. The spiral arm is defined by $\rho = \rho_0 + \alpha\varphi$, where ρ_0 is the feeding segment length, α is the spiral constant and φ is the winding angle. The thin wire approximation has been adopted, piecewise sinusoidal current pulses have been employed and a delta gap voltage source has been used for excitation.

The input impedance has been calculated in two cases: first, assuming the antenna is placed in the third layer that has a relative permittivity of $\varepsilon_{r3} = 2$ and a thickness of 0.75 cm, and then when the spiral is located at the second layer. In both cases, the antenna has been positioned at the interface between the two layers. The permittivities of the first and second layers have been assumed to be $\varepsilon_2 = \varepsilon_1 = \varepsilon_0$ and the radius of the PEC spherical core chosen as 5 cm, that is, $1\lambda_o$ at an operating frequency of 6 GHz. The spiral has been modeled using $\rho_0 = 0.163$ cm, $\alpha = 0.0623$ cm/rad, a maximum winding angle of 12.4 rad and a wire radius of 0.02 cm [17].

Fig. 2 shows the convergence of the input impedance when the infinite summation of (2) is truncated using asymptotic extraction approach compared to the case when the summation is implemented directly, that is, with no use of asymptotic extraction. It is evident from these results that the required number of terms to truncate the series has been reduced from over 100 to approximately 25 when the proposed

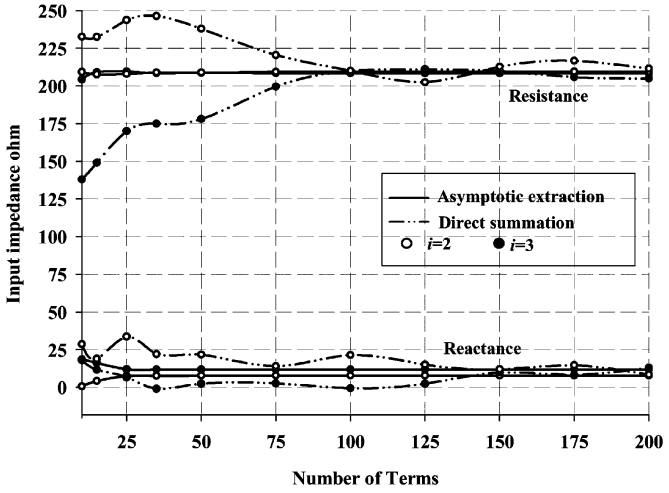

Fig. 2. Convergence of the input impedance of a spherical spiral using a PEC spherical core radius of $1\lambda_o$ when the antenna is placed at the dielectric interface between a spherical substrate and free space, where i refers to the index of the antenna layer.

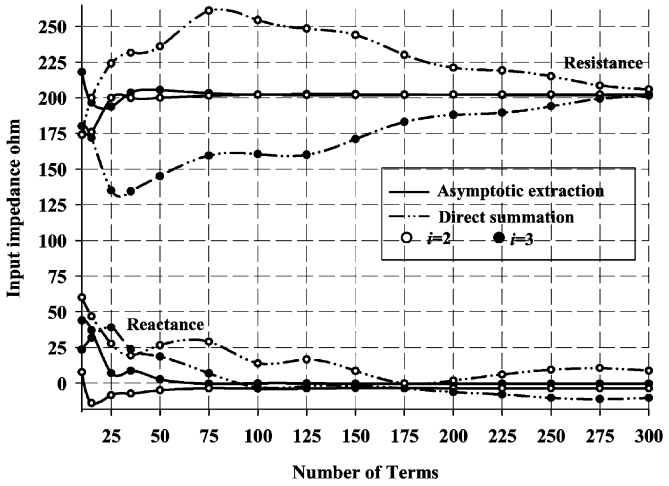

Fig. 3. Convergence of the input impedance of a spherical spiral positioned at dielectric interface using a PEC spherical core radius of $3\lambda_o$.

model is employed. As expected, the convergent input impedance is the same whether the antenna is positioned in the second or the third layer as long as it is located at the interface, with a slight difference in the imaginary part owing to the numerical computations of Hankel functions using different arguments.

The required number of terms increases as the size of the sphere is increased, hence a structure with a larger sphere radius has been investigated. Fig. 3 presents the impedance convergence when a PEC spherical core of radius $3\lambda_o$ is used, where, again, it can be seen that a convergent solution has been achieved using approximately 75 terms when asymptotic extraction is employed, compared with more than 300 terms when the summation is implemented directly. It should be mentioned that the impedance converges to $203 - j2\ \Omega$ compared to $208 - j4\ \Omega$ for an identical planar spiral when the antenna is located at the third layer.

The convergence of the input impedance at the presence of a dielectric superstrate is then studied using $\varepsilon_{r3} = 2.2$, $\varepsilon_{r2} = 4.2$, $a_3 = 12$ cm, $a_2 = 12.8$ cm and $a_1 = 13.4$ cm at a frequency of 5 GHz. The spiral parameters have been chosen as those reported in [18] for an equivalent spiral in an identical planar media, that is, $\rho_0 = 0.253$ cm,

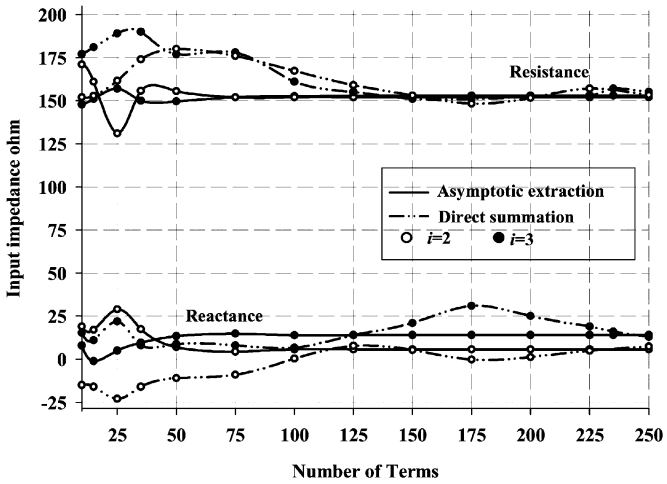

Fig. 4. Convergence of the input impedance of a spherical spiral located at an interface of a dielectric substrate and a superstrate using a PEC spherical core radius of $2\lambda_o$.

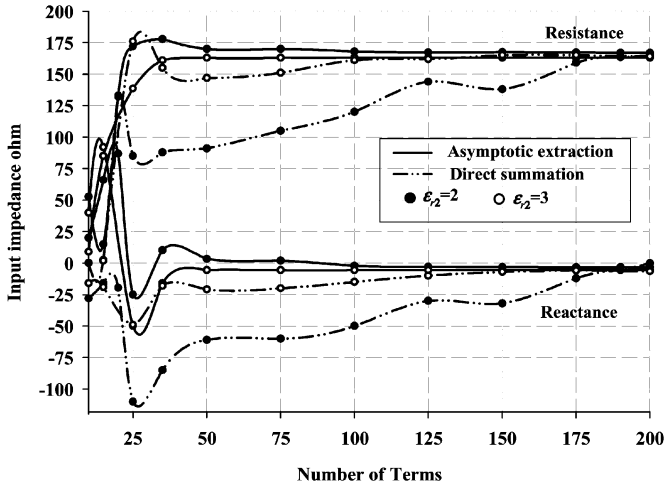

Fig. 5. Convergence of the input impedance of a conformal probe-fed patch antenna using $\varepsilon_{r3} = 3$ and different superstrate permittivities at the corresponding resonance frequencies.

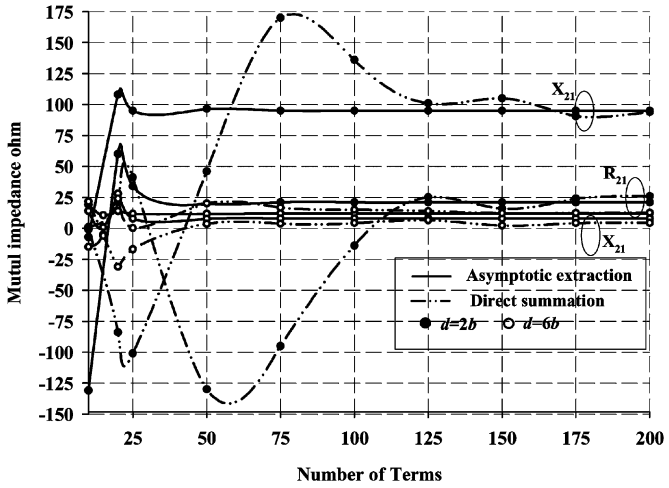

Fig. 6. Convergence of the mutual impedance between two identical circular patches with a radius of b and an arc separation distance of d between their centers.

$\alpha = 0.097$ cm/rad and a maximum winding angle of 12.4 rad. In this example the antenna has been assumed to be placed first in the second layer, i.e., the spherical superstrate, and then in the third layer, i.e., the spherical substrate, at the interface between those layers. The input impedance convergence is presented in Fig. 4 where a significant acceleration in the convergence is again accomplished when the asymptotic extraction is employed.

The capability of the model to analyze structures with electrically thin spherical layers has been examined by modeling a probe-fed circular patch antenna that is printed on a 0.2 cm spherical substrate and covered by a superstrate with a similar thickness. The PEC spherical core radius and the substrate permittivity have been chosen as $a_3 = 10$ cm and $\varepsilon_{r3} = 3$, respectively. The patch antenna has been modeled using an arc radius of 1.88 cm, and it has been fed using a probe that is located at an arc distance of 0.94 cm from its center. The patch and the probe have been placed in the third layer with the patch antenna positioned at the dielectric boundary between the second and the third layers. Further, the structure has been analyzed using different superstrate permittivities: the first is $\varepsilon_{r2} = 2$ and the second is $\varepsilon_{r2} = 3$, which results in two resonance frequencies of 2.54 GHz and 2.49 GHz, respectively. Employing similar substrate and superstrate permittivities facilitates evaluation of the effectiveness of the model when the patch is close to, but not located at, a dielectric interface. Fig. 5 illustrates the convergence of the input impedance at the accordant resonance frequencies, where it can be observed that a substantially reduced number of expansion terms are sufficient to accomplish convergence when asymptotic extraction is employed. It can be seen from these results that the convergence of the direct summation improved noticeably when the antenna is shifted from the dielectric boundary.

A two-element array has been analysed using the aforementioned microstrip antenna and sphere parameters, where the mutual coupling has been evaluated using $\varepsilon_{r2} = 2$ at a frequency of 2.54 GHz, that is, the array is located at an interface between thin layers. The convergence has been investigated in two configurations: first using an arc distance of $d = 2b$ between the centers of the patches, and then using a larger arc distance of $6b$, where b is the patch radius. The mutual impedance has been obtained from the solution of the MoM block-Toeplitz impedance matrix, where 200 terms have been added for the self-term matrix entries to ensure convergence, while the added number of terms for the mutual coupling entries has been varied as shown in Fig. 6. Mutual coupling results show that asymptotic extraction expedites convergence considerably for small as well as large angular separation distances.

The numerical results illustrate the advantages of employing the introduced solution in the analysis of geometries that consist of electrically thick as well as thin spherical layers. Compared to other acceleration techniques, asymptotic extraction avoids the computation overheads that are associated with traditional approaches such as Watson and Shanks transformations [5]–[7]. The algorithm enhances the computation efficiency significantly for arbitrarily angular distances between the source and field points, which is different from a previously reported methodology that is suitable for larger separation distances [8]. Furthermore, in contrast to the solutions introduced in [9], [10], there is no restriction on the sphere size, number of layers, or antenna orientation. However, the accomplished improvement and the effectiveness of the model depend on the proximity of the antenna to a dielectric interface. This is owing to the rapid decline of the extracted quasi-static images' contributions as the antenna is moved away from a dielectric boundary, where the direct summation of the infinite series converges using a considerably reduced number of spherical eigenmodes.

IV. Conclusion

An asymptotic extraction procedure has been established to accelerate the convergence of the infinite series of DGF in a multilayered spherical media. The superiority of the introduced model has been demonstrated in the MoM analysis of conformal antennas located at a spherical surface, where various configurations have been investigated. Early truncation of the series reduces the computation time considerably and eliminates the numerical limitations associated with a large-order Hankel and Bessel functions.

In this study, attention is given to the problem of source and field points located in the same layer. The presented procedure can be followed to formulate asymptotic Green's functions when the source and observation points are in different layers. The computations speed can be enhanced further by adopting the closed-form expressions reported in [11], [12] in conjunction with the proposed procedure in the analysis of a number of spherical antennas geometries.

Appendix A

When $n \rightarrow \infty$, the spherical Bessel and Hankel functions can be approximated using the principal asymptotic expressions [19]

$$j_n(kr) \approx \sqrt{\frac{1}{2kr\,(2n+1)}}\left(\frac{ekr}{2n+1}\right)^{n+(1/2)} \tag{A1}$$

$$h_n^{(2)}(kr) \approx j\sqrt{\frac{2}{kr\,(2n+1)}}\left(\frac{ekr}{2n+1}\right)^{-n-(1/2)} \tag{A2}$$

which lead to

$$\frac{j_n(k_f a_{f+1})}{j_n(k_f a_f)} \approx \left(\frac{a_{f+1}}{a_f}\right)^n \tag{A3}$$

$$\frac{h_n^{(2)}(k_f a_f)}{h_n^{(2)}(k_f a_{f+1})} \approx \left(\frac{a_{f+1}}{a_f}\right)^{n+1} \tag{A4}$$

and

$$\frac{dj_n(kr)}{dr} \approx \frac{n}{r} j_n(kr) \tag{A5}$$

$$\frac{dh_n^{(2)}(kr)}{dr} \approx -\frac{(n+1)}{r} h_n^{(2)}(kr) \tag{A6}$$

$$\frac{d\left(rj_n(kr)\right)}{dr} \approx (n+1)\, j_n(kr) \tag{A7}$$

$$\frac{d\left(rh_n^{(2)}(kr)\right)}{dr} \approx -nh_n^{(2)}(kr). \tag{A8}$$

Since $n \gg 1$, (A7) can be expressed as

$$\frac{d\left(rj_n(kr)\right)}{dr} \approx nj_n(kr). \tag{A9}$$

Appendix B

The following recurrence formulas can be employed to compute the scattering DGF coefficients [3]

$$A_{M,N}^{(f+1)s} = \frac{A_{M,N}^{fs}}{T_{Ff}^{V,H}} + \frac{R_{Ff}^{V,H}}{T_{Ff}^{V,H}} C_{M,N}^{fs} - \delta_{(f+1)}^{s} \tag{B1}$$

$$B_{M,N}^{(f+1)s} = \frac{B_{M,N}^{fs}}{T_{Ff}^{V,H}} + \frac{R_{Ff}^{V,H}}{T_{Ff}^{V,H}} D_{M,N}^{fs} + \frac{R_{Ff}^{V,H}}{T_{Ff}^{V,H}} \delta_f^s \tag{B2}$$

$$C_{M,N}^{(f+1)s} = \frac{R_{Pf}^{V,H}}{T_{Pf}^{V,H}} A_{M,N}^{fs} + \frac{C_{M,N}^{fs}}{T_{Pf}^{V,H}} \tag{B3}$$

$$D_{M,N}^{(f+1)s} = \frac{R_{Pf}^{V,H}}{T_{Pf}^{V,H}} B_{M,N}^{fs} + \frac{D_{M,N}^{fs}}{T_{Pf}^{V,H}} + \frac{\delta_f^s}{T_{Pf}^{V,H}}. \tag{B4}$$

With the aid of (3) explicit asymptotic expressions can be derived for the aforementioned coefficients. For instance, in the four layers geometry shown in Fig. 1, it can be proved that

$$B_N^{11}\big|_a = -\left\{w_1 + w_2\left(\frac{a_2}{a_1}\right)^{2n+1} + w_3\left(\frac{a_3}{a_1}\right)^{2n+1} + w_1 w_2 w_3\left(\frac{a_3}{a_2}\right)^{2n+1}\right\}\frac{j_n(k_1 a_1)}{h_n(k_1 a_1)} \tag{B5}$$

where the first three terms correspond to local reflections at the dielectric interfaces and the last term accounts for multiple reflections, which is generally smaller than the other terms hence it can be neglected. Further, as $a_{i+2} < a_i$ for any spherical geometry the third term of (B5) declines rapidly by a factor $(a_{i+2}/a_i)^{2n+1}$ as $n \rightarrow \infty$. Therefore, substituting (A1)–(A2) into the first and second terms of (B5) gives

$$B_N^{11}\big|_a = -w_1\frac{j_n(k_1 a_1)}{h_n(k_1 a_1)} - w_2\frac{j_n(k_1 a_2)}{h_n(k_1 a_2)}. \tag{B6}$$

Following a similar procedure, asymptotic representations of all the coefficients can be accomplished.

References

[1] C. T. Tai, *Dyadic Green's Functions in Electromagnetics Theory*. Scranton, PA: Intext Educational, 1971.

[2] W. C. Chew, *Waves and Fields in Inhomogeneous Media*. New York: Van Nostrand, 1990.

[3] L. W. Li, P. S. Kooi, M. S. Leong, and T. S. Yeo, "Electromagnetic dyadic Green's function in spherically multilayered media," *IEEE Trans. Microw. Theory Tech.*, vol. 42, pp. 2302–2310, Dec. 1994.

[4] R. F. Harrington, *Time Harmonic Electromagnetic Fields*. New York: Mc Graw-Hill, 1961.

[5] G. M. Watson, "The diffraction of electric waves by the earth," *Proc. Royal Society*, vol. 95, pp. 83–99, 1919.

[6] D. Shanks, "Non-linear transformation of divergent and slowly convergent sequences," *J. Math. Phy.*, vol. 34, pp. 1–42, 1955.

[7] F. M. Tesche, A. R. Neureuther, and R. E. Stovall, "The analysis of monopole antennas located on a spherical vehicle: Part 2, numerical and experimental results," *IEEE Trans. Electromagn. Compat.*, vol. 18, pp. 8–15, Feb. 1976.

[8] V. I. Okhmatovski and A. C. Cangellaris, "Efficient calculation of the electromagnetic dyadic Green's function in spherical layered media," *IEEE Trans. Antennas Propag*, vol. 51, pp. 3209–3220, 2003.

[9] B. D. Milovanovic, "Numerical analysis of radial thin-wire antenna in presence of conducting sphere," *Elec. Lett.*, vol. 16, no. 15, pp. 611–612, Jul. 1980.

[10] L. W. Li, T. Fei, Q. Wu, and T. S. Yeo, "Convergence acceleration for calculating radiated fields by a vertical electric dipole in the presence of a large sphere," in *Proc. IEEE Antennas Propag. Soc. Int. Symp.*, Jul. 2005, vol. 2B, pp. 117–120.

[11] K. W. Leung, "General solution of a monopole loaded by a dielectric hemisphere for efficient computation," *IEEE Trans. Antennas Propag.*, vol. 48, pp. 1267–1268, Aug. 2000.

[12] K. W. Leung, "Analysis of the zonal and rectangular slots on a conducting spherical cavity'," *IEEE Trans. Antennas Propag.*, vol. 49, pp. 1739–1745, Dec. 2001.

[13] D. R. Jackson and N. G. Alexopoulos, "An asymptotic extraction technique for evaluating Sommerfeld-type integrals," *IEEE Trans. Antennas Propag.*, vol. AP-34, pp. 1467–1470, Dec. 1986.

[14] M. J. Tsai, F. D. Flaviis, O. Fordham, and N. G. Alexopoulos, "Modeling planar arbitrarily shaped microstrip elements in multilayered media," *IEEE Trans. Microw. Theory Tech.*, vol. 45, pp. 330–337, Mar. 1997.

[15] C. Chen, W. E. McKinzie, III, and N. G. Alexopoulos, "Stripline-fed arbitrarily shaped printed-aperture antennas," *IEEE Trans. Antennas Propag.*, vol. 45, pp. 1186–1198, Jul. 1997.

[16] J. Sun, C. F. Wang, L. W. Li, and M. S. Leong, "Further improvement for fast computation of mixed potential Green's functions for cylindrically stratified media," *IEEE Trans. Antennas Propag.*, vol. 52, pp. 3026–3036, Nov. 2004.

[17] S. K. Khamas, "Moment method analysis of an Archimedean spiral printed on a layered dielectric sphere," *IEEE Trans. Antennas Propag.*, vol. 56, pp. 345–352, Feb. 2008.
[18] S. K. Khamas, P. L. Starke, and G. G. Cook, "Design of a printed spiral antenna with a dielectric superstrate using an efficient curved segments moment method with optimization using marginal distributions," in *Proc. Inst. Elect. Eng. Microw, Antennas Propag.*, Aug. 2004, vol. 151, pp. 315–320.
[19] M. Abramowitz and I. A. Stegun, "Handbook of mathematical functions with formulas," in *Graphs, and Mathematical Tables*. Washington, DC: Government Printing Office, 1964.

Miniature Internal Penta-Band Monopole Antenna for Mobile Phones

Chia-Ling Liu, Yi-Fang Lin, Chia-Ming Liang, Shan-Cheng Pan, and Hua-Ming Chen

***Abstract*—A compact T-slit monopole antenna with slotted ground plane in the mobile phone for penta-band operation is proposed. In this configuration, the antenna comprises a T-slit monopole printed on the top ungrounded portion of an FR4 substrate of small size of $47 \times 5.4\ \mathrm{mm}^2$ and a slotted ground plane etched on the back side of the substrate of size of $47 \times 10\ \mathrm{mm}^2$. In addition, an inverted-L copper strip is soldered to the end edge of the monopole for extending the electrical length of the antenna for GSM band; that is, the proposed antenna occupies a small volume of $47 \times 10 \times 5\ \mathrm{mm}^3$ inside the mobile phone and is suitable to operate as an internal antenna. By controlling the related parameters, the proposed antenna can resonates at different operating bands to cover GSM850/900 and DCS/PCS/UMTS operations independently.**

***Index Terms*—Mobile phone, penta-band, T-slit monopole antenna.**

I. Introduction

Recently with the rapid development of cellular communication, various types of antennas for mobile phones have been extensively presented and the trend of the mobile phones is getting smaller and slimmer because of the consumer's needs and the multiplicity of functions. Conventional internal antennas for the mobile phones applications are generally in forms of monopole antennas because it can provides a wide impedance bandwidth [1]–[6]. These monopole antennas generally use two separate resonant paths of different lengths operated at their quarter-wavelength modes to cover the mobile phone's operating bands.

In this communication, we present a promising compact penta-band monopole antenna with an occupied volume of $10 \times 47 \times 5\ \mathrm{mm}^3$ in the mobile phone to operate GSM (824–894/890–960 MHz), DCS (1710–1880 MHz), PCS (1850–1990 MHz), and UMTS (1920–2170 MHz) bands. The proposed antenna is easily printed on a thin substrate at low cost and fabricated by a bending metal plate shown a very low profile of 5 mm. The low profile of the antenna allows it very promising to be embedded inside the mobile phone as an internal antenna. In order to determine the performance of varying design parameters on bandwidth and resonance frequency, parametric study is carried out using simulation software HFSS and experimental results. Detailed design considerations of the proposed antenna are described in this article.

Manuscript received March 11, 2009; revised August 30, 2009. First published December 28, 2009; current version published March 03, 2010. This work was supported by the National Science Council of Taiwan under Contract NSC 97-2221-E-151-010.

C.-L. Liu, Y.-F. Lin, C.-M. Liang, and H.-M. Chen are with the Institute of Photonics and Communications, National Kaohsiung University of Applied Sciences, Kaohsiung 807, Taiwan (e-mail: linyf@cc.kuas.edu.tw; hmchen@cc.kuas.edu.tw).

S.-C. Pan is with the Department of Computer and Communication, Shu-Te University, Yen Chau, Kaohsiung 824, Taiwan.

Color versions of one or more of the figures in this communication are available online at http://ieeexplore.ieee.org.

Digital Object Identifier 10.1109/TAP.2009.2039309

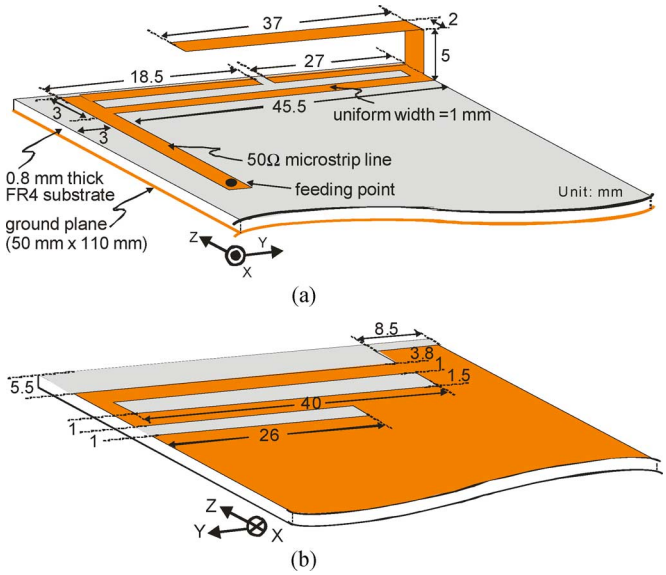

Fig. 1. Configuration of the T-shaped slit monopole antenna with slotted ground plane for mobile phone application.

II. Antenna Configuration

Fig. 1 shows the configuration of the T-slit monopole antenna with slotted ground plane for mobile phone application. A 0.8-mm thick FR4 substrate of relative permittivity 4.4 and of size $110 \times 50\ \mathrm{mm}^2$ is used as the system circuit board with a ground plane of the same size. The dimensions of the system circuit board and ground plane considered here are practical for general mobile phones. In Fig. 1(a), the antenna comprises a T-slit monopole printed on the top ungrounded portion of an FR4 substrate of small size $47 \times 5.4\ \mathrm{mm}^2$ and a slotted ground plane etched on the back side of the substrate of size $47 \times 10\ \mathrm{mm}^2$. In this study, an inverted-L copper strip is soldered to the end edge of the monopole for extending the electrical length of the antenna for GSM band. For the inverted-L copper strip, it comprises a horizontal section of size $37 \times 2\ \mathrm{mm}^2$ and a vertical section of size $5 \times 2\ \mathrm{mm}^2$. In addition, a T-slit is etched on the monopole radiator to realize two major current paths and achieving an additional resonant mode. A 50-Ω microstrip feed line printed on the top side of the system circuit board has a length of 35 mm and a width of 1.5 mm. Fig. 1(b) shows the dimensions of the pattern of the ground plane on the back side of the substrate. The pattern comprises a narrow straight slot and a narrow slit. By varying the length of the slit, the various coupling energy between the feed line and the pattern in the ground plane can results in another excited resonant mode. Detailed dimensions of the antenna are given in Fig. 1.